

# A novel FFNN-AHO hybrid predictive model for enhancing the performance of jet-cooled PVT system

Mohamed A. Essa<sup>1,2</sup>, Alaa M. Rashad<sup>3</sup>, Ahmed Y. Hatata<sup>4,5</sup>

<sup>1</sup>Department of Mechanical Engineering, College of Engineering, Shaqra University, Dawadmi, Saudi Arabia

<sup>2</sup>Department of Mechanical Power Engineering, Faculty of Engineering, Zagazig University, Zagazig, Egypt

<sup>3</sup>Department of Civil Engineering, College of Engineering, Shaqra University, Dawadmi, Saudi Arabia

<sup>4</sup>Department of Electrical Engineering, College of Engineering, Shaqra University, Dawadmi, Saudi Arabia

<sup>5</sup>Department of Electrical Engineering, Engineering College, Mansoura University, Mansoura, Egypt

## Article Info

### Article history:

Received Feb 1, 2024

Revised Feb 22, 2024

Accepted Feb 26, 2024

### Keywords:

Archerfish hunting optimizer

Artificial neural network

Electrical efficiency

Overall efficiency

PVT

Thermal efficiency

## ABSTRACT

Photovoltaic-thermal (PVT) systems are common in the conversion of solar energy to electrical and thermal energy. The performance of such systems depends on the environmental conditions in which these systems are applied. This paper presents a parametric study of a jet-cooling PVT system with a staggered distribution of the jets. A feedforward neural network (FFNN) is proposed as a novel predictive model for analyzing the characteristics of the PVT system and its thermal and electrical performance. Moreover, a novel optimization algorithm called archerfish hunting optimizer (AHO) is applied to obtain the optimal structure and elements of the proposed FFNN. The PVT system variables considered as inputs to the FFNN-AHO model are flow rate, wind speed, solar irradiance, and ambient temperature. The average temperature of the PV reaches a maximum of 45.84 °C, and the maximum temperature un-uniformity reaches to 3.59 °C. The studied PVT system achieved maximum electrical, thermal, and overall efficiencies of 14.23%, 54.43%, and 68.1%, respectively. Moreover, the results demonstrate that the FFNN-AHO hybrid model provides highly accurate PVT system performance prediction. The correlation coefficient between the actual and predicted data is close to 1, indicating a strong correlation and confirming the reliability and effectiveness of the FFNN-AHO model.

This is an open access article under the [CC BY-SA](https://creativecommons.org/licenses/by-sa/4.0/) license.



## Corresponding Author:

Mohamed A. Essa

Department of Mechanical Engineering, College of Engineering, Shaqra University

Dawadmi, 11911 Riyadh, Saudi Arabia

Email: maessa@su.edu.sa

## 1. INTRODUCTION

Photovoltaic (PV) systems are common solar energy conversion systems in the market. Recently, PV thermal (PVT) systems have been proposed for producing thermal energy with the electrical energy produced from PV. The PVT system raises the PV electrical efficiency ( $\eta_e$ ) because of the cooling. Furthermore, it produces thermal energy as a byproduct. This effect was led to achieve a maximum overall efficiency ( $\eta_o$ ) of up to 80% for the PVT system [1]. The PVT systems differs in the cooling technique and fluids [2], [3]. So, the following paragraphs introduces the up-to-date research considering cooling techniques and fluids in PVT systems.

The PVT systems use either active or passive cooling techniques in the thermal module attached to the PV. The active technique applies forced convection for the heat transfer from the PV to the heat transfer fluid (HTF), while the passive technique applies free convection. Passive techniques rely on extending the heat

transfer surface, often by heat sinks, to achieve a greater heat removal rate from the PV module. Fins attached to the backside of the PV system as a heat sink was investigated using aluminium fins with ten different orientations [4]. The staggered array of the fins with a  $0.014 \text{ m}^2$  area achieved the highest exergy and energy efficiencies of 10.91%, and 11.55%, respectively. Longitudinal S-shaped fins heat sink was investigated by [5]. This technique achieved an enhancement in  $\eta_e$  by 0.42%. The achieved  $\eta_e$  and thermal efficiency ( $\eta_t$ ) reached 13.98% and 49.5%, respectively. Discontinuity of the heat sinks was investigated in comparison with the continuous heat sinks [6]. The disconnected heat sink achieved  $7 \text{ }^\circ\text{C}$  lower PV temperature with an enhancement of 2.96%. Broken versus continuous ribs were investigated, as well, in a PVT system with water as the HTF [7]. The continuous  $45^\circ$  V-shaped ribs achieved the highest heat removal rate. The system achieved an improvement in  $\eta_e$  by up to 1.5%, while  $\eta_t$  reached 53%. The effect of the cooling air stream temperature was investigated using underground cooling [8]. An underground depth of 1 m was used in the system with different flow rates of the air stream. The achieved temperature decrease in the PV panel was  $13 \text{ }^\circ\text{C}$  under a flow rate of  $0.0288 \text{ m}^3/\text{s}$ . This enhancement in the PV temperature improved its  $\eta_e$  by 18.9%.

Heat sink with U-shaped fins construction cooling was compared with the water flow cooling for the PV modules by [7]. An improvement in the produced energy by 7% and 10.2% was achieved using heat sinks and water cooling, respectively. This referred to the decrease in the PV panel's maximum temperature by  $17 \text{ }^\circ\text{C}$  and  $20 \text{ }^\circ\text{C}$ . A similar comparative study was conducted to investigate the effect of the water-cooling system compared to pin fins separately [9]. A  $2^\circ$  inclination converging channel achieved the minimum temperature deviation of  $0.92 \text{ }^\circ\text{C}$  through the PV panel. This system improved  $\eta_e$  by 36.1%. Forced convection water cooling using in-contact spray jets was investigated by [10]. The sprayed water with a flow rate of  $0.1425 \text{ LPS}$  achieved a reduction in the maximum PV temperature by  $26.4 \text{ }^\circ\text{C}$  on sunny days. This enhanced the annual energy productivity by 6.1%. A two-sided cooling technique was applied to achieve better cooling for the PV. An upper and lower side cooling by the forced flow of water and air, respectively, was investigated by [11]. The two-sided cooling technique achieved a PV temperature reduction by  $15 \text{ }^\circ\text{C}$  and enhanced  $\eta_e$  by up to 5.7%. The value of  $\eta_o$  of this PVT system reached 85.3%. The flow channel in which the HTF flows inside the PVT system has had several shapes and performances. Rectangular and arc cross-section channel geometries in the PVT systems were investigated [12]. The arc channel achieved an enhancement in  $\eta_e$  by 0.45% and 0.95% in comparison with rectangle channel system and PV system without cooling. The arc cross-sectional channels achieved  $\eta_t$  of 65.95%. Moreover, corrugated channels with shark dorsal shape and V-shape in the PVT module were investigated [13]. This system reached a maximum  $\eta_t$  of 10.5%.

Heat transfer parameters in the thermal module were investigated for performance enhancement in a PVT system using water as the HTF [14]. Variable Reynolds number was considered by varying the tube diameter and the flow rate. Both  $\eta_t$  and  $\eta_e$  increased with the Reynolds number. Within the tested parameters, the overall efficiency ( $\eta_o$ ) reached a maximum value of 59.3%. Twisted tape inserts in the riser tubes of the thermal module were used in a PVT system for heat transfer enhancement [15]. The PV temperature decreased using the twisted tabs. As a result, the energy efficiency experienced a boost of 28.4%. Thermosiphon was used for thermal energy extraction from the PV at the backside [16]. The operating temperature of the PV decreased by 17%, and  $\eta_e$  was improved by 7.3%. An unglazed PVT system utilizing water and nanofluid was investigated separately with a thermal absorber tube and serpentine coil PVT system [17]. A decrease in PV temperature by  $23.7 \text{ }^\circ\text{C}$  and  $15 \text{ }^\circ\text{C}$  was achieved by utilizing nano-fluid and water, respectively. The value of  $\eta_o$  of the nano-fluid case was found to be higher than that of the water-cooling case by 21%. A comparative study for PVT-solar thermal (ST) and PV-ST systems was conducted [18]. For high ambient temperatures and solar radiation, the PVT-ST demonstrated superior performance compared to the PV-ST. A PVT system was proposed based on a thermal collector with a PV panel that partially covers it [19]. The harvested power increased by 31.24% and experienced a reduction of 35.07% when compared to the PV system only. An examination was conducted on an air-heated PVT system that incorporated baffles to enhance heat transfer [20]. The best baffles arrangement achieved enhancements of 4.3% and 12.9% in  $\eta_t$  and  $\eta_e$ , respectively. A triangular-shaped thermal module with air as HTF was used with a PVT [21]. The system achieved an enhancement of 36.97% and 2.59% in  $\eta_t$  and  $\eta_e$ , respectively. An experimental investigation was conducted using PV cooling with thermoelectric module PVT-TE [22]. They found that the overall systems efficiency can reach 72.1% without considering pumping losses.

In recent times, machine learning techniques, particularly artificial neural network (ANN), have demonstrated their effectiveness in modelling the performance of thermal and electrical systems, such as heat exchangers and PV systems. Consequently, ANN methodologies have gained significant popularity in accurately predicting the dynamic performance of PVT systems under diverse external and internal conditions. This encompasses factors like fluid mass flow rate, climate fluctuations, and system design parameters, which have been recognized as relevant considerations [23]. Various ANN models including, radial-basis function ANN, adaptive neuro-fuzzy inference system, and FFNN, were utilized to model PVT systems incorporating nanofluids as a heat transfer fluid [24]. Moreover, the ANNs, along with the particle swarm optimization

technique, were employed to determine the efficiency of the PV module and the outlet temperature of the collector fluid. The results demonstrated the capability of these models to predict the desired parameters [24]. Furthermore, a genetic algorithm-back propagation neural networks model was employed to improve the performance of parabolic trough solar collectors (PTSCs) by minimizing heat loss and maximizing energy output and overall efficiency [25]. The ANN models were employed to predict the characteristics of nano-fluid-based solar collectors. These models utilized inputs such as reduced temperature difference, collector length, collector depth, nano-fluid concentration, and flow rate to predict collector efficiency and Nusselt number [26].

Additionally, FFNNs were utilized in various PVT models to enhance the efficiency of different configurations, such as PVT connected with thermoelectric cooler (PVT-TEC) systems [27]. These models enabled the prediction of electrical, thermal, and overall exergy efficiencies, as well as average fluid temperature. Furthermore, ANN models were used to enhance the energy generation of PVT systems based on nano-phase change materials (nano-PCMs), SiC-water, and nanofluids [28]. Inputs such as ambient temperature and solar irradiance were utilized to predict energy generation using self-organizing feature maps and multilayer perceptron networks. The evaluation of these models demonstrated favourable results in terms of R2 value, root mean squared error (RMSE) value, MSE value, and trend accuracy. Two distinct ANN models were proposed to predict various PVT performance parameters, including outlet temperature, cell temperature, and exergy, thermal, and electrical efficiencies [29]. These models were specifically designed for PVT systems using hexagonal boron nitride/water nanofluid as the cooling fluid. A FFNN was employed to predict the efficiency of PVT. Inputs such as cell temperature and solar irradiance were utilized, and the model was trained using climatic data from various weather conditions. The developed FFNN model exhibited high accuracy in estimating efficiency parameters [30].

Other studies employed methods such as least squares support vector machine and ANN to model PVT systems and predict their thermal and electrical efficiencies [23]. The findings showed that the LS-SVM approach demonstrated superior performance in this context. A comprehensive review and comparison of various ANN models, including LSTM, SOFM, SVM, SOVM, MLP, GFF, and RNN, was conducted to assess their data prediction capabilities in PVT collectors [27]. The results indicated that a specific transverse zone with moderate to high irradiation levels was favourable for implementing solar systems. Various ANN models, including LS-SVM and adaptive neuro-fuzzy inference system, were presented to optimize the efficiency of nano-coolant PVT systems [31]. These models utilized inputs such as irradiation intensity and nanofluid flow rate. The ANFIS model demonstrated superior performance in predicting efficiency, achieving low MSE, RMSE, and high R<sup>2</sup> values.

As concluded from the literature, the active cooling methods showed excellent performance, especially with water as the cooling fluid. The nano-fluid showed even higher heat transfer rates. However, the pumping power of the nano-fluids is high due to the frictional losses. It does not benefit the PVT systems' overall performance if counted for in the overall efficiency. One of the best cooling techniques for the PV panels found is the jet cooling. However, some parts of the jet-cooling still need more investigation especially for the design and range of the test parameters used. In the current study, a parametric study for a multiple jet with single outlet cooling for the PV as a compact PVT system was conducted. The orientation of the jets is a staggered distribution. The parameters that will be considered in this study are HTF flow rate, Ambient temperature, wind speed, and solar radiation intensity. Furthermore, an FFNN is proposed as a novel predictive model for analyzing the characteristics of the PVT system and its electrical and thermal performance. Moreover, a novel optimization algorithm, AHO, is applied to calculate the optimal structure and elements of the proposed FFNN. The FFNN-AHO hybrid prediction model is trained by data from the CFD model. The results of the study are analyzed considering the maximum un-uniformity and the average temperature of the PV module,  $\eta_t$ ,  $\eta_e$ , and  $\eta_o$  of the PVT system.

The following sections contain a detailed description of methodology used for the CFD and the FFNN-AHO models used with validating data in the methods section. Then a results and discussion section present a detailed exploring and discussion for the CFD results considering the temperature distribution and uniformity on the PV panel and different efficiencies of the system followed by a detailed discussion of the FFNN-AHO model validity and accuracy. Furthermore, the conclusion section presents the outstanding conclusions from this work. Finally, a section for the related future work that can be conducted in this area is presented.

## 2. METHOD

The PV module considered in this paper is a 50 W polycrystalline module (EGE-50P-36). The thermal module is considered to be an aluminum box attached to the PV backside with a thermal paste. The PVT module under study has dimensions of 515×675×22.2 mm<sup>3</sup> with the specifications from [32]. The jets are directed normally to the PV inside the thermal module domain. The jet distribution is considered, as shown in Figure 1. Lv and Lh express the vertical and horizontal distance between the jets. The diameter of the jet is dj.

The jet diameter is considered to be 5 mm for all the cases. The jet distances have been considered as  $L_v=168.57$  mm and  $L_h=171.67$  mm, while the jet distance to the wall is considered as 7.5 mm.

**2.1. Numerical model**

A numerical model is built for the proposed PVT system. The model has a tilt angle of 45°. Ansys ICEM program is utilized for grid and geometry generation according to the dimensions indicated in Figure 1. Ansys fluent solver is used in this paper for the CFD, heat transfer, radiation modelling, and simulation using the finite volume method. A simple algorithm is used for the velocity-pressure coupling. RNG K-ε model is used for the turbulence modelling. The standard discretization scheme is applied for the pressure equation, the momentum and energy equations utilize the second-order upwind scheme, whereas the turbulence equations employ the first-order upwind scheme. A steady flow solution is obtained by setting a convergence criterion of 1E-4 for the momentum, continuity, and turbulence equations. For the energy and radiation equations, a convergence criterion of 1E-6 is applied. The flow rate range for the cooling HTF is 0.14:1.27 LPM, with wind speeds of 0 and 3 m/s, ambient temperatures of 293 and 308K, and solar irradiance range of 400:1200 W/m<sup>2</sup>. The equations considered in the numerical simulation understudy are momentum, continuity, energy in solid and liquid mediums, and the RNG k-ε turbulence for which the detailed description can e found in [33].

A hexahedrons structured mesh is constructed for the present study using the Ansys ICEM meshing tool. A mesh sensitivity test is implemented to study the effect of the mesh density on the final solution. Figure 2 indicates the average PV temperature with increasing mesh density considering flow rate of 1.414 L/min and 1,000 W/m<sup>2</sup> irradiance. It is found that as the number of elements reaches 1.6 million, the temperature variation can be neglected. So, the mesh considered in the simulations of the present test cases contains 1.6 million elements.

The specifications related to the different boundaries are illustrated in Figure 3. The irradiance is assumed to be perpendicular on the PV, while the PV panel is considered inclined by 30° on the horizontal. The entered cooling fluids are jets with the distribution illustrated. The outlet is a longitudinal slot with a width of 3 mm at the bottom of the thermal module. The temperature of the cooling HTF is considered equal to the ambient temperature ( $T_{amb}$ ). The external wind speeds are considered to be 0 and 3 m/s, causing convection coefficient values of 2.8 and 11.8 W/m<sup>2</sup>. K, respectively [13]. To verify the validity of the current model, a comparison is made between its predictions and the experimental results presented in [34]. The comparison between the numerical data and the experimental is shown in Figure 4.

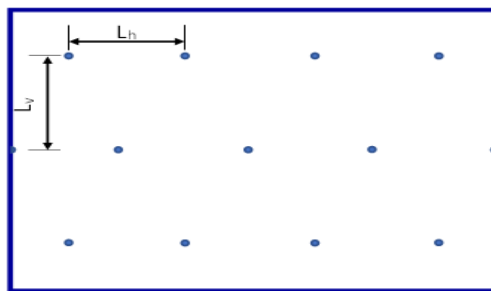


Figure 1. Jets orientation in the thermal module

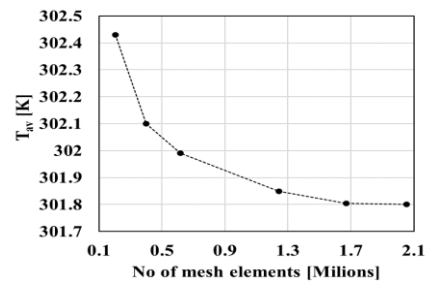


Figure 2. Grid sensitivity for the mesh

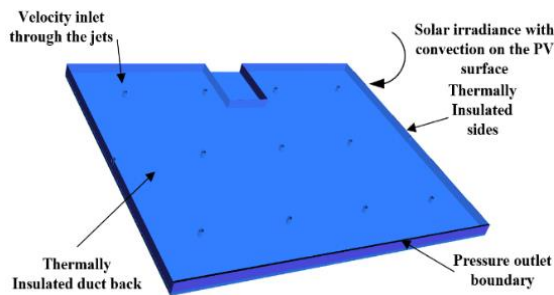


Figure 3. The PVT model with boundary conditions

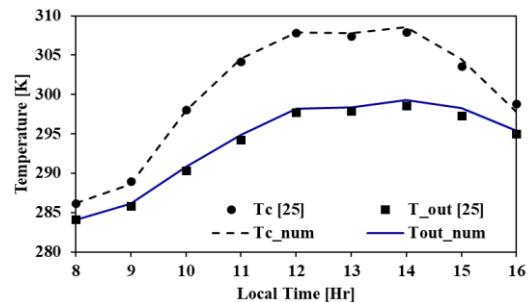


Figure 4. Numerical data validation

As can be observed from Figure 4, a maximum ARE of 4.1% was found between the simulation and the experimental data. The performance parameters considered in this research are  $\eta_t$ ,  $\eta_e$ ,  $\eta_o$ ,  $T_{av}$ ,  $\Delta T$ , and  $T_{out}$  where  $T_{av}$  expresses the area-weighted average of the PV top surface temperature. This parameter is vital for judging the effectiveness of the cooling technique used. Another important parameter is the temperature non-uniformity index of the PV module ( $\Delta T$ ), which expresses the variation of the PV module temperature. In this study, it is the difference between the maximum and minimum PV temperature.  $\Delta T$  is important for the PVT application to judge the effective distribution of the cooling technique over the PV. This is because the high value of this index causes cracks in the PV module due to thermal stresses over the long-term operation [35]. The definition of the  $\eta_t$ ,  $\eta_e$  can be found in [36]. The Overall efficiency  $\eta_o$  considers the pumping power ratio ( $P_{Pr}$ ), which expresses the power exerted in the HTF pumping relative the solar power input as:

$$P_{Pr} = \dot{V} * \Delta p / P_{in} \tag{1}$$

where  $\Delta p$  is the pressure loss of the HTF pumpig [Pa],  $\dot{V}$  is the HTF flow rate [m<sup>3</sup>/s], and  $P_{in}$  is the solar power input to the system [W]. The overall efficiency  $\eta_o$  is expressed as in (2).

$$\eta_o = \eta_e + \eta_t - P_{Pr} \tag{2}$$

**2.2. ANN**

The ANN is a type of artificial intelligence technique designed to mimic the neural networks found in the human brain, enabling analysis, computation, and information processing. Unlike traditional programming, it utilizes training and learning algorithms to solve problems. It consists of multiple layers, including the input, hidden, and output layers, with each layer comprising a collection of neurons that serve as the primary computational units. The optimal number of hidden layers and neurons depends on the problem complexity. Each neuron in a layer receives inputs ( $I_1, I_2, \dots$ ) from the neurons in the preceding layer, along with a bias term ( $B$ ), which are then multiplied by weights ( $\omega$ ). The neuron's output ( $O$ ) is calculated by implementing the activation function ( $\xi$ ) to the weighted sum of the inputs, as defined in (3) [36], [37].

$$O = \xi[\sum_{i=1}^n (\omega_i I_i + B)] \tag{3}$$

The activation function is associated with each neuron to compute its output. Popular activation functions for hidden layers include sigmoid/logistic and rectified linear unit. For the output layer, linear, and binary Step activation functions are commonly used [37].

This paper introduces a proposed FFNN for modelling the thermal solar PV (PVT) system. The FFNN model is capable of predicting various performance parameters of the PVT system, including PV temperature, thermal efficiency  $\eta_t$ ,  $\eta_e$ , and  $\eta_o$ . The input layer of the FFNN is designed to receive initial data in the form of a vector consisting of ambient temperature, mass flow rate, convection coefficient, and solar irradiance. This input layer comprises four neurons, with each neuron corresponding to one of the input parameters. Similarly, the output layer consists of six neurons, representing  $\eta_t$ ,  $\eta_e$ ,  $\eta_o$ ,  $T_{av}$ ,  $\Delta T$ , and  $T_{out}$ .

During the training process, the proposed FFNN learns to predict the actual values of the PVT performance parameters by adjusting the connection weights between neurons in different layers. The objective of the training process is to reduce the errors between the actual and predicted outputs by iteratively adjusting the weights. To evaluate the effectiveness of the training process, the MSE is calculated as a measure of the disparity between the predicted and actual outputs. The MSE is utilized to correct the biases and connection weights between the layers, ensuring improved accuracy and performance [37].

$$MSE = \frac{1}{n} \sum_{i=1}^n (A_i - T_i)^2 \tag{4}$$

Where  $n$  is the training pattern numbers and  $A_i$  and  $T_i$  represent the predicted output and measured values, respectively. The objective function can be written as (5).

$$OF = Min. \left[ \frac{1}{n} \sum_{i=1}^n (A_i - T_i)^2 \right] \tag{5}$$

Figure 5 depicts the ultimate configuration of the proposed FFNN, where the inputs consist of ambient temperature, convection coefficient, mass flow rate, and solar irradiance. Additionally, the output parameters are visually presented in Figure 5. The optimal number of hidden neurons is determined by leveraging a novel optimization approach known as archerfish hunting optimizer (AHO). This technique is employed to acquire appropriate values for the weights and biases. Consequently, a hybrid model combining AHO and FFNN (FFNN-AHO) is established to derive the PVT system characteristics.

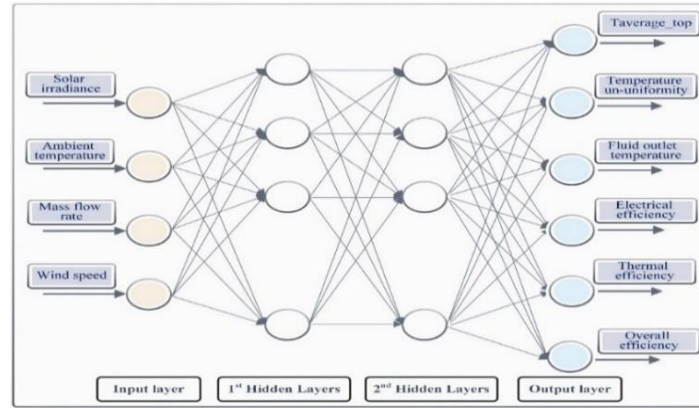


Figure 5. Proposed FFNN structure for modelling PVT system

### 2.3. AHO

In this paper, a novel metaheuristic approach AHO is utilized to calculate the optimal structure of the FFNN for predicting and modelling the PVT system performance. This technique is inspired by the hunting behavior of archerfish, which mimics actions such as jumping and shooting water to target insects. When hunting insects, the archerfish employs two methods: it either propels a strong stream of water to strike the insect or jumps towards it when it is in close proximity. This behavior is mathematically simulated and referred to as AHO. The AHO method requires the configuration of three parameters: population size, attraction rate between the archerfish and insects, and the angle at which the system switches between exploitation and exploration phases. To implement the AHO technique, the AHO parameters need to be initialized first, including the population size and the number of archerfish. The initial positions of the  $i$ th archerfish,  $P(i,0)$ , can be denoted by [38], [39].

$$P(i, 0) = [(p_1^L + \sigma_1(p_1^U - p_1^L)), \dots, (p_d^L + \sigma_d(p_d^U - p_d^L))] \quad (6)$$

Where  $p_1^U$  and  $p_1^L$  represent the lower and upper bounders of the archerfish location.  $\sigma_1, \dots, \sigma_d$  are random numbers between 0 and 1.

#### 2.3.1. Shooting behavior (exploration phase)

During this phase, the motion of water droplets shot by the archerfish is modelled using a general ballistic trajectory. The launch speed,  $v$ , can be calculated based on the perception angle,  $\phi$ , and the acceleration of gravity,  $\delta$ . The archerfish,  $j$ , targets the insect and shoots water, causing the insect to fall into the water. Then the archerfish  $i$ th at iteration  $(t+1)$  moves towards the fallen insect using [38];

$$P(i, t + 1) = -(P(i, t) - P_{in}(i, t)) e^{-\|P_{in}(j, t) - P(i, t)\|_2^2} + P(i, t) \quad (7)$$

where  $t$  is the number of iterations,  $P(i, t)$  and  $P(i, t + 1)$  represent the positions of archerfish  $i$ th at iteration  $t$  and  $t+1$  and  $\| \cdot \|^2$  is Euclidean norm. The position of the insect can be obtained by (8);

$$P_{in}(i, t) = P(i, t) + \left(0, \dots, \frac{v^2}{2\delta} \times \sin 2\phi, \dots, 0\right) + \epsilon \quad (8)$$

where  $\epsilon$  is a vector of random numbers in the range  $[-0.5, 0.5]$ .

#### 2.3.2. Jumping behavior (exploitation phase)

During this phase, the archerfish engages in hunting the insect by jumping towards it. Just like in the previous phase, the motion of the archerfish is calculated by the launch speed, perception angle, and acceleration of gravity. The movement of the  $i$ th archerfish towards the insect as it hunts it down can be described by [38].

$$P(i, t + 1) = -(P(i, t) - P_{in}(i, t)) e^{-\|P_{in}(i, t) - P(i, t)\|_2^2} + L(i, t) \quad (9)$$

Additionally, the position of the insect can be modelled using;

$$P_{in}(i, t) = P(i, t) + \left(0, \dots, \frac{v^2}{2\theta} \times \sin 2\phi, \dots, \frac{v^2}{2\theta} \times \sin^2 \phi, \dots, 0\right) + \epsilon \tag{10}$$

if the archerfish position,  $P(i, t)$ , has not been modified during the iterations, a new position for  $P(i, t)$  will be generated using in the (11) and (12) [39];

$$P(i, t + 1) = P(i, t) + \sigma \left[ \frac{p_1}{v_1^{(1/\beta)}}, \dots, \frac{p_d}{v_d^{(1/\beta)}} \right] \tag{11}$$

$$\begin{cases} p_i \sim f_n(0, \gamma^2), \gamma = \left( \frac{\Gamma(\beta+1) \times \sin(\frac{\pi\beta}{2})}{\Gamma(\frac{\beta+1}{2}) \times 2^{(\frac{\beta-1}{2})} \times \beta} \right)^{\frac{1}{\beta}}, i \in \{1, \dots, d\} \\ v_i \sim f_n(0, \gamma'^2), \gamma' = 1, i \in \{1, \dots, d\} \end{cases} \tag{12}$$

where  $f_n(\mu, \gamma)$  represents the normal distribution function with a mean  $\mu$  and standard deviation  $\gamma$ . The gamma function is denoted by  $\Gamma$ , and the power law index  $\beta$  is set to 1.5. Figure 6 provides a visual representation of the flowchart outlining the proposed AHO technique.

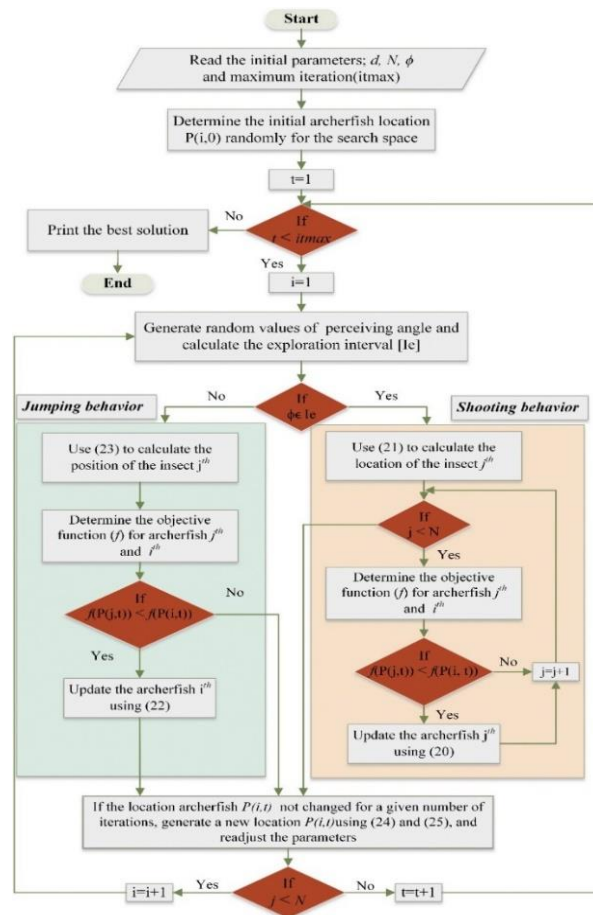


Figure 6. Procedure for constructing the optimal FFNN model using the AHO technique

### 2.4. Optimal FFNN model structure

For this study, an FFNN with two hidden layers, as depicted in Figure 5, is chosen. Different networks with varying numbers of hidden layers were tested, revealing that increasing the number of hidden layers beyond two had only a minor impact on the predictive accuracy. The input data for the proposed FFNN is divided randomly into three groups: testing, validation, and training. The training group comprises 70% of the input data, while the validation and testing groups consist of 15% each. To calculate the optimal number of

neurons in the two hidden layers, the network is trained, and the MSE between the FFNN outputs and the actual values of the performance parameters of the PVT system ( $\eta_t$ ,  $\eta_e$ ,  $\eta_o$ ,  $T_{av}$ ,  $\Delta T$ , and  $T_{out}$ ) is minimized. Also, during the training process, the connection biases and weights between the different layers are selected using the proposed AHO technique. Additionally, the activation function for the output and hidden layers is established. Figure 6 provides an illustration of the procedure for constructing the FFNN model optimally and the training algorithm for predicting the performance parameters of the PVT system.

The detailed steps of the procedure are as follows:

- Create the training data for the proposed FFNN from  $\eta_t$ ,  $\eta_e$ ,  $\eta_o$ ,  $T_{av}$ ,  $\Delta T$ , and  $T_{out}$ . Subsequently, transfer this data to the MATLAB program for further processing.
- Randomly generate initial values for the parameters of the proposed FFNN, including activation function, biases, weights, and the number of hidden neurons. Additionally, define the population size.
- Construct the proposed FFNN with the determined numbers of neurons in the hidden layers.
- Define the MSE as the objective function and calculate its values for each search agent in the search space.
- Utilize the proposed AHO technique, as illustrated in Figure 6, to train the proposed FFNN and determine the best values of parameters that minimize the MSE.
- Repeat steps 3 to 6 until the desired accuracy or the maximum number of iterations is reached.

### 3. RESULTS AND DISCUSSION

In this section, the performance of the PVT system under study and the ANN model are explored under different study parameter ranges. The temperature variation with the study parameters and the temperature un-uniformity are presented first. In the second subsection, the energy performance considering the electrical, thermal, and overall efficiency is discussed. The third subsection discusses the ANN model results and precession.

#### 3.1. Variation of $T_{av}$ and $\Delta T$

The efficiency of the cooling technique is identified principally by the average temperature of the PV module,  $T_{av}$ . Figure 7. shows the variation of  $T_{av}$  and  $\Delta T$ . It is observed that the cooling flow rate positively affects the  $T_{av}$ , especially at high radiation intensities. The ambient temperature plays an important role in increasing the value of  $T_{av}$ , especially with a high external convection coefficient as observed from the Figures 7(a) and 7(c). At the highest cooling flow rate of 1.27LPM,  $T_{av}$  reaches a range of 300.57 to 302.01 K at a radiation intensity of 1,200 W/m<sup>2</sup>. Compared to the lowest flow rate, at which  $T_{av}$  is 312.33 K, the highest cooling achieves a decrease in  $T_{av}$  by 11.76 K, which is equivalent to 3.7% on K basis and 42.6% on °C basis, considering the highest radiation intensity tested. The value of  $T_{av}$  reaches a maximum of 318.84 K under the highest cooling with the highest radiation intensity as observed from the Figure 7(d) due to high value of  $T_{amb}$  and lower external coefficient of convection. However, it is observed that the performance of Figures 7(b) and 7(c) are similar due to the low  $T_{amb}$  with low h value, and high  $T_{amb}$  with high h value, respectively. Regarding the variation of  $\Delta T$ , it is observed from Figure 7 that the value of  $\Delta T$  decreases with the increase of the cooling flow rate and the decrease of the radiation intensity. It decreases under low ambient temperatures with a high external convection coefficient, as well, as in Figure 7(a). At the highest radiation intensity of 1,200 W/m<sup>2</sup>, the value of  $\Delta T$  reaches 3.02 K and 3.59 K at Figures 7(a) and 7(d), respectively, at the highest cooling flow rate. At low radiation intensities, the value of  $\Delta T$  is lower than 1.5K, with the highest value reached at the highest  $T_{amb}$  and highest h vales indicated in Figure 7(c), considering the applied ranges of the test parameters. Figure 7(b) indicates higher values of  $\Delta T$  like that of Figure 7(c).

#### 3.2. Variation of the electrical and thermal efficiencies

The variation of the  $\eta_e$  and  $\eta_t$  of the PVT system is shown in Figure 8. The value of  $\eta_e$  is inversely proportional to the PV temperature. It is observed that the value of  $\eta_e$  increases with the increase of the flow rate and decreases under high intensity of radiation. It is observed that the effect of the cooling on  $\eta_e$  is higher at the highest radiation intensity of 1,200 W/m<sup>2</sup>.  $\eta_e$  has the lowest value of 12.8% at the highest  $T_{amb}$  and lowest h vales indicated in Figure 8(d), and the highest value of 13.85% at the lowest  $T_{amb}$  and highest h vale indicated in Figure 8(a). This achieves a 7% enhancement of  $\eta_e$  at highest radiation. Although  $\eta_e$  is higher at lower radiation intensities, the effect of cooling enhances  $\eta_e$  from 13.89% in Figure 8(c) to 14.23% in Figure 8(b), achieving an enhancement of 2.4%.

The variation of  $\eta_t$  under the test parameters variation is depicted in Figure 8 as well. It is observed that  $\eta_t$  increases with the solar radiation and the cooling flow rate. For the test parameter ranges in this study, the value of  $\eta_t$  reaches a maximum value of 54.43% at the highest  $T_{amb}$  and highest h vales indicated in Figure 8(c) achieved at the maximum cooling flow rate and maximum irradiance power. On the contrary of  $\eta_e$ ,



$\eta_t$  is proportional to the ambient temperature. At the maximum cooling flow rate,  $\eta_t$  reaches a minimum value of 13.4% at the lowest  $T_{amb}$  and highest  $h$  value indicated in Figure 8(a), which is achieved at the minimum radiation power. The value of  $\eta_t$  is enhanced for higher  $T_{amb}$  if compared to the lowest  $T_{amb}$  values as indicated in Figures 8(b) and 8(d), respectively.

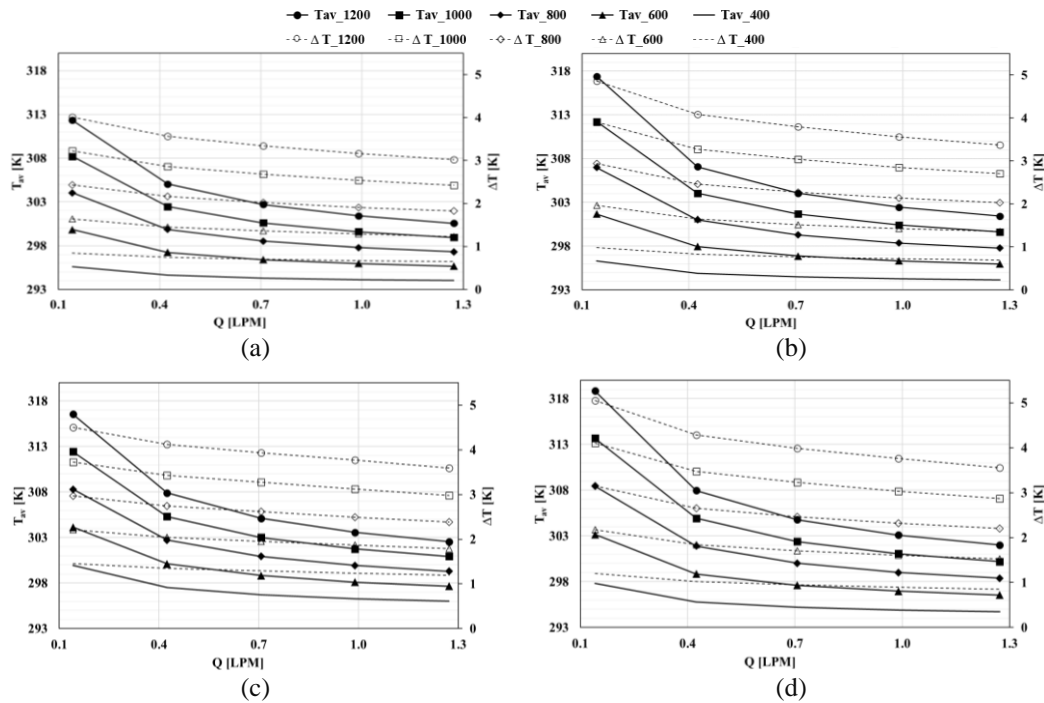


Figure 7. Variation of  $T_{av}$  and  $\Delta T$  for; (a)  $T_{amb}=293K$  and  $h=11.8 W/m^2.K$ , (b)  $T_{amb}=293 K$  and  $h=2.8 W/m^2.K$ , (c)  $T_{amb}=308K$  and  $h=11.8 W/m^2.K$ , and (d)  $T_{amb}=308K$  and  $h=2.8 W/m^2.K$

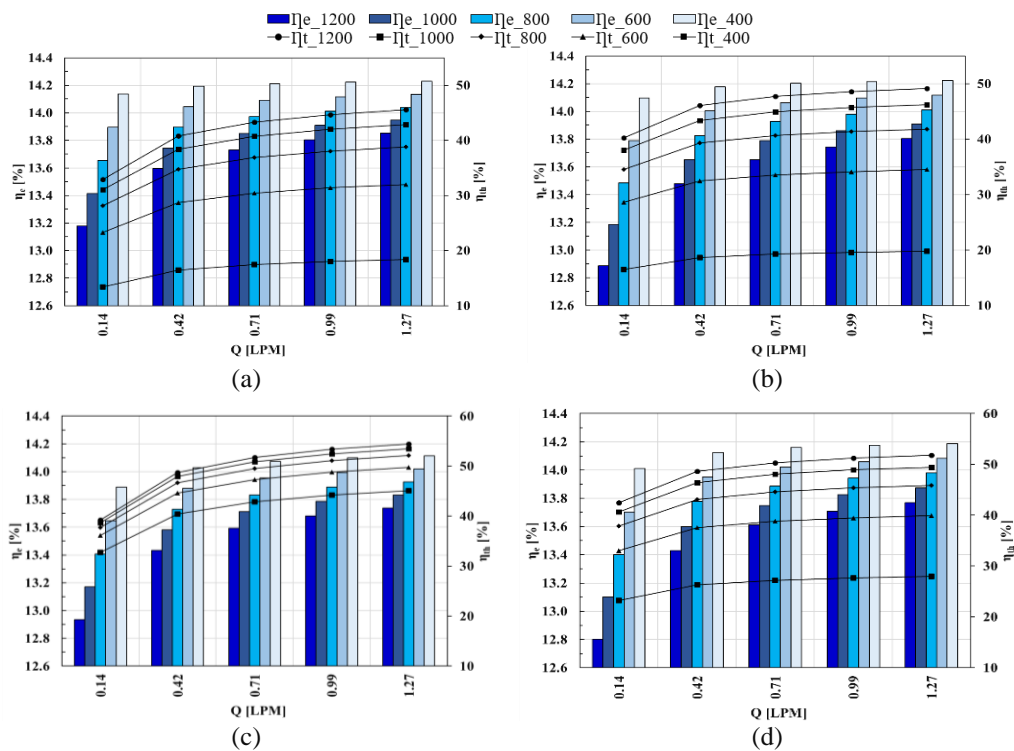


Figure 8. Variation of  $\eta_e$  and  $\eta_t$  for; (a)  $T_{amb}=293K$  and  $h=11.8 W/m^2.K$ , (b)  $T_{amb}=293K$  and  $h=2.8 W/m^2.K$ , (c)  $T_{amb}=308K$  and  $h=11.8 W/m^2.K$ , and (d)  $T_{amb}=308K$  and  $h=2.8 W/m^2.K$

### 3.3. Variation for the overall efficiency

For the different effects of the test parameters on the thermal and electrical efficiencies, it was important to investigate the variation of the overall system performance through  $\eta_o$ . This value is calculated according in (2) considering the power losses consumed in the cooling fluid pumping. Figure 9 illustrates the variation of  $\eta_o$  over the test parameter ranges. It is observed that the behaviour of  $\eta_o$  is more similar to that of  $\eta_t$  as it is proportional to the cooling flow rate, ambient temperature, and radiation intensity. This refers to the larger value of  $\eta_t$  compared to  $\eta_e$ , for most of the test cases. The value of  $\eta_o$  reaches a maximum of 68.17% found in Figure 9(c), which is achieved at the highest radiation intensity, highest cooling flow rate, highest ambient temperature, and the highest external convection coefficient. The lowest value of  $\eta_o$  reaches 27.54% found in Figure 9(a) due to higher thermal losses, under the test parameter ranges in this study. The value of  $\eta_o$  is enhanced for higher  $T_{amb}$  if compared to the lowest  $T_{amb}$  values as indicated in Figures 9(b) and 9(d), respectively.

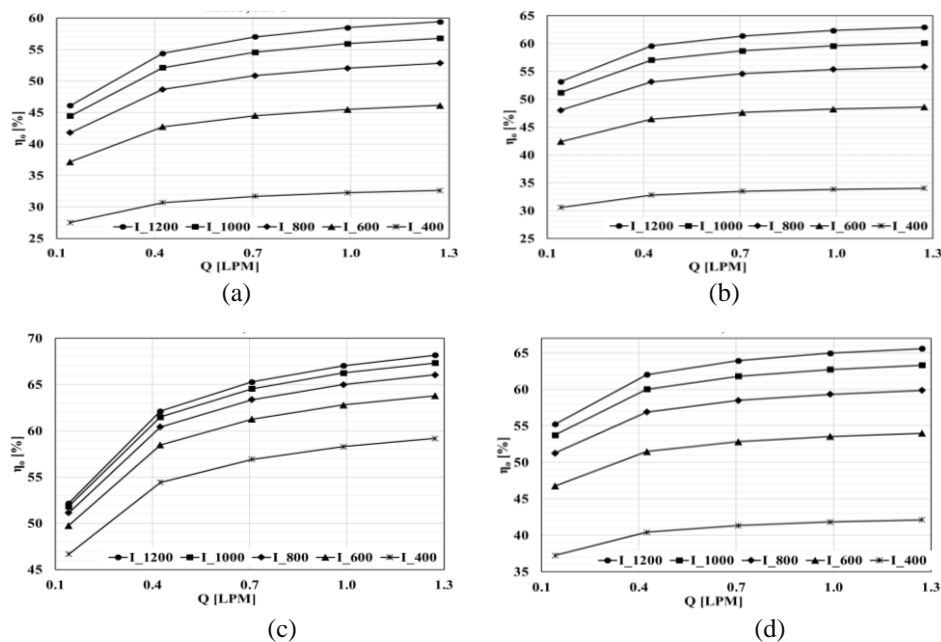


Figure 9. Overall efficiency of the PV module for; (a)  $T_{amb}=293K$  and  $h=11.8 W/m^2.K$ , (b)  $T_{amb}=293K$  and  $h=2.8 W/m^2.K$ , (c)  $T_{amb}=308K$  and  $h=11.8 W/m^2.K$ , and (d)  $T_{amb}=308K$  and  $h=2.8 W/m^2.K$

### 3.4. Proposed FFNN-AHO results

In this study, the performance of the PVT system is modelled using the FFNN. The training of the proposed FFNN is conducted through two approaches: the trial-and-error method and the AHO method. The implementation and execution of the FFNN are done using the MATLAB program. The training datasets comprise around 100 patterns, representing various cases to ensure a comprehensive coverage of the study. These datasets are utilized to train the FFNN.

The results of the regression factor, denoted as R, for the FFNN trained with the AHO method (optimized) are depicted in Figure 10. Figure 10(a) showcases the regression factor during the training process, while Figure 10(b) portrays the regression factor during the validation process of the FFNN-AHO model. Lastly, Figure 10(c) illustrates the regression factor during the testing process of the FFNN-AHO model. They indicate that the model exhibits good conversion and fitting performance based on the demonstrated regression factor. Furthermore, when the AHO technique is applied to optimize the parameters of the FFNN, the resulting regression factors are closer to 1 than other methods.

Figure 11 presents a comparison between the PVT performance parameters ( $\eta_t$ ,  $\eta_e$ ,  $\eta_o$ ,  $T_{av}$ ,  $\Delta T$ , and  $T_{out}$ ) obtained from measurements and the outputs generated by the FFNN-AHO when utilizing all the available data sets (100 patterns). Figures 11(a) and 11(b) depict the values of the actual  $T_{av}$  and  $\Delta T$  of the solar cells and the predicted values from the FFNN-AHO model. As illustrated from the figures the errors between the actual and predicted values are very small, where the MSEs for the  $T_{av}$  and  $\Delta T$  are  $2.27 \times 10^{-4}$  and  $2.48 \times 10^{-4}$ . In Figure 11(c), the graph illustrates the level of agreement between the actual  $T_{out}$  values and the values estimated

by the FFNN-AHO model with an MSE value of  $2.45 \times 10^{-4}$ . Furthermore, the ability of the FFNN-AHO model to predict the PVT efficiencies ( $\eta_t$ ,  $\eta_e$ , and  $\eta_o$ ) are demonstrated in Figures 11(d), 11(e), and 11(f), respectively. The MSEs for predicting the  $\eta_t$ ,  $\eta_e$ , and  $\eta_o$  reach  $2.39 \times 10^{-4}$ ,  $2.86 \times 10^{-4}$ , and  $2.93 \times 10^{-4}$ , respectively. These figures emphasize the similarity between the actual and the predicted values obtained from the FFNN-AHO model, indicating the validity and accuracy of the proposed neural network model. Moreover, the proposed FFNN, trained using the AHO method, contributes to minimizing the disparity between the actual values and the FFNN-AHO outputs, resulting in a significantly smaller error compared to using the FFNN trained with the trial-and-error method. The AHO method successfully reduces the average MSE to a value of  $2.56 \times 10^{-4}$ .

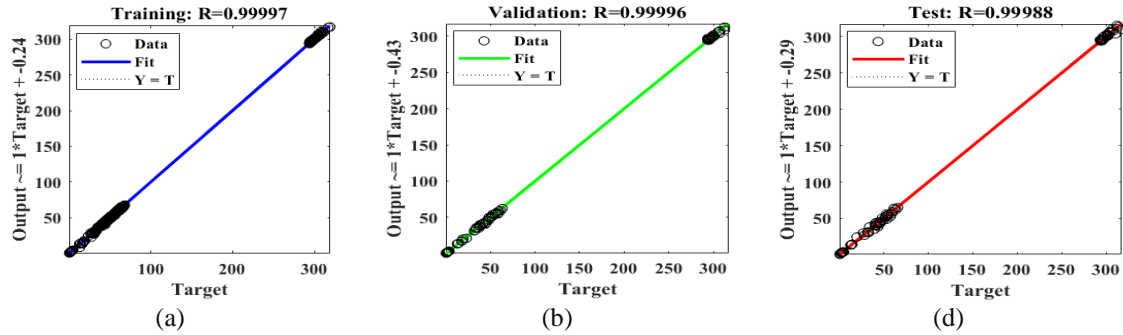


Figure 10. Regression factor, R, obtained after applying the AHO method for; (a) regression factor, R, for the training dataset, (b) regression factor, R, for the validation dataset, and (c) regression factor, R, for the testing dataset

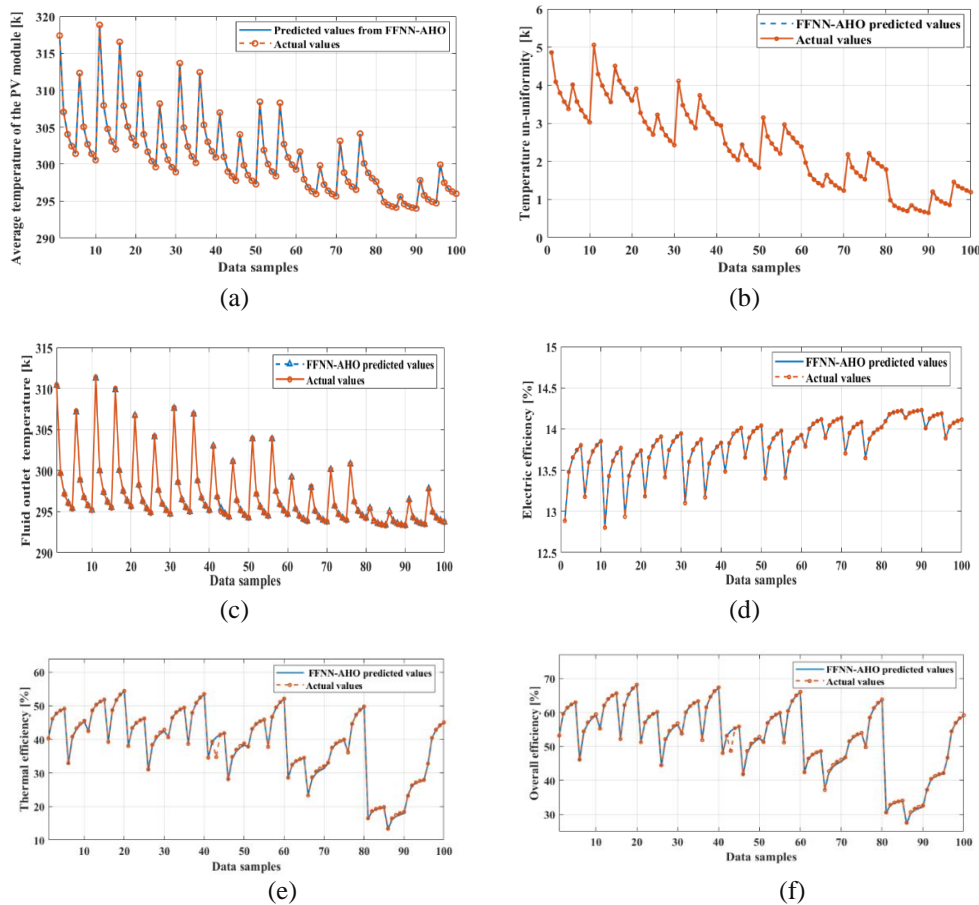


Figure 11 Comparison between the actual PVT performance parameters and the FFNN-AHO model outputs for; (a) average temperature of the PV module, (b) temperature un-uniformity of the PV module, (c) fluid outlet temperature, (d) electrical efficiency, (e) thermal efficiency, and (f) overall efficiency

After achieving the desired performance, the number of hidden neurons and their respective weights are fixed. Subsequently, the proposed FFNN is evaluated using various independent test patterns. These test patterns are distinct from the datasets utilized during the network's training phase. To assess the extrapolation capability of the proposed FFNN-AHO model, 16 specific patterns are chosen for testing it as shown in Figure 12. These patterns are deliberately excluded from the FFNN's training process and are representative of different scenarios within the problem. Figures 12(a) and 12(b) display the actual  $T_{av}$  and  $\Delta T$  values of the solar cells, along with the predicted values generated by the FFNN-AHO model. These figures demonstrate that the errors between the actual and predicted values are minimal. Figure 12(c) illustrates the level of agreement between the actual  $T_{out}$  values and the values estimated by the FFNN-AHO model. Additionally, Figures 12(d), 12(e), and 12(f) showcase the capability of the FFNN-AHO model to predict the PVT efficiencies ( $\eta_t$ ,  $\eta_e$ , and  $\eta_o$ ) respectively. Thus, the optimized FFNN-AHO model demonstrates a high level of accuracy in predicting the performance parameter values of the PVT system, not only for the trained data but also for non-trained data. The best construction of the proposed FFNN is (4-23-16-6).

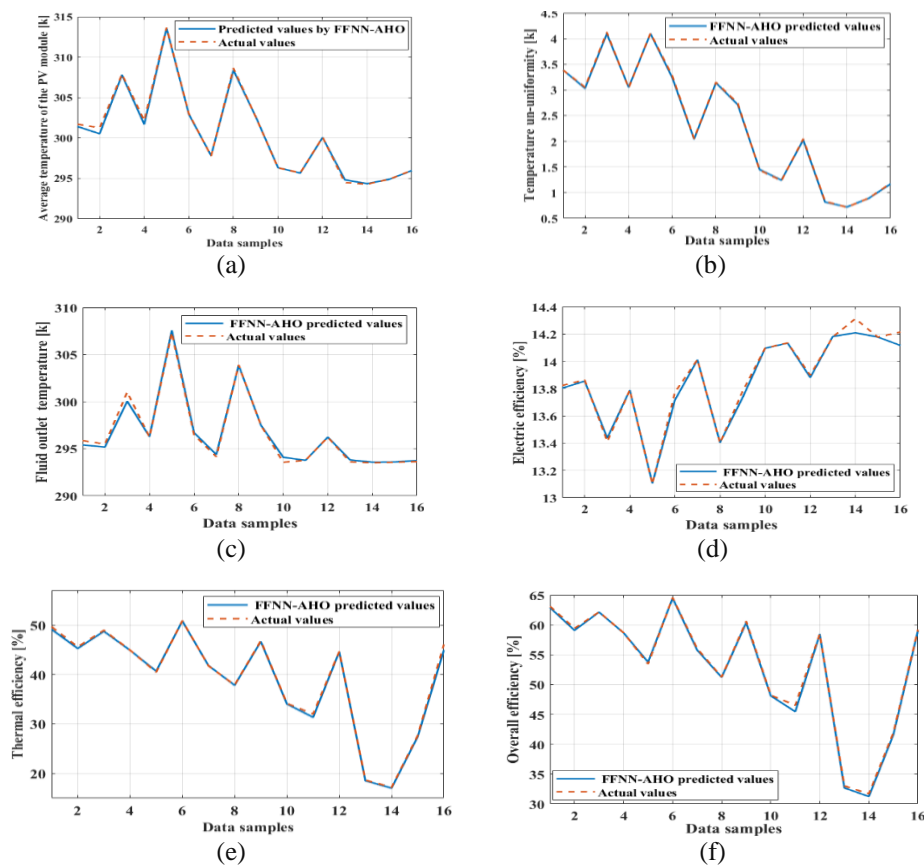


Figure 12. Comparison between the actual PVT performance parameters and the FFNN-AHO model outputs for tested data patterns for; (a) average temperature of the PV module, (b) temperature un-uniformity of the PV module, (c) fluid outlet temperature, (d) electrical efficiency, (e) thermal efficiency, and (f) overall efficiency

### 3.5. Comparative analysis

A comparison of the presented cooling technique with other techniques in the literature is introduced in Table 1. It is observed that there are some systems achieving higher overall efficiencies of the present research of 68.1%. However, some of these systems are complicated and introduce upper and lower surface cooling as [11]. The present cooling techniques presents an advantage of compactness and eas of manufacturing over this in [11]. Other systems as in [16] presented efficiencies reaching 90%. However, these systems did not account for the hydraulic pumping losses of the fluid. Moreover, the hydraulic losses for the nanofluid are higher than pure water for the dissolved particles and the high viscosity. Because of this comparison, the authors think that the present PVT system is promising for future development including enhancement of heat transfer using baffels and fins for consideration in the cogeneration systems.

Table 1. Comparison of the PVT systems performance with recent studies

References	Cooling technique	Fluid	$\eta_e$ (%)	$\eta_t$ (%)	$\eta_o$ (%)
Gomaa <i>et al.</i> [7]	Open box with baffles	Water	13	53	61
Elminshawy <i>et al.</i> [8]	Serpentine	Air	16	NA	NA
Bevilacqua <i>et al.</i> [10]	Sparay jets	Water	15.5	NA	NA
Lebbi <i>et al.</i> [11]	Upper and lower channels	Water with air	13.2	50	85
Pang <i>et al.</i> [12]	Channels	Water	16.9	39.8	65.9
Shen <i>et al.</i> [13]	Corrugated channel	Water	10.3	10.5	NA
Hassan <i>et al.</i> [14]	Serpentine with absorber plate	Water	14.8	44.5	59
Kalateh <i>et al.</i> [15]	tubes with twisted tapes	Water	11.88	72	NA
Chiang <i>et al.</i> [16]	Serpentine with absorber plate	Water	15.5	66.5	80*
		nanofluid	18.8	78	95*
Song <i>et al.</i> [20]	Channels with baffles	Air	13.6	52.8	NA
Choi and Choi [21]	Corrugated channel	Air	16.8	45	NA
Present study	Jet cooling in a compact module	Water	14.23	54.43	68.1

\*Indicates that the overall efficiency does not account for the hydraulic losses exerted on the HTF.

The performance evaluation of the proposed MFFNN-AHO models in predicting the PVT system's performance metrics ( $\eta_t$ ,  $\eta_e$ ,  $\eta_o$ ,  $T_{av}$ ,  $\Delta T$ , and  $T_{out}$ ) is conducted using the mean squared error (MSE) index. Table 2 presents the MSE values for the proposed FFNN-AHO model, alongside the values obtained from other methods such as RBFNN-GTO [36], RBFNN trained with the backpropagation algorithm (BP), RBFNN trained with trained with PSO method and FFNN trained with PSO method [24]. It is evident from the table that the proposed MFFNN-AHO model exhibits superior performance compared to the other methods. This can be attributed to the ANN's strong capability to model nonlinear relationships and handle complex problems by utilizing input-output datasets, combined with the AHO's ability to obtain optimal network parameters and structure.

Table 2. Evaluation of the MFFNN-AHO model performance compared to various neural networks

Model	MSE
RBFNN-BP	5.2442×E-04
RBFNN-PSO	6.4656×E-04
FFNN-PSO	7.9831×E-04
RBFNN-GTO	3.7613×E-04
Proposed FFNN-AHO	2.5613×E-04

#### 4. CONCLUSION

A parametric study with an ANN prediction model for a jet-cooling PVT system was conducted. The parameters ranges used in this study were 400-1200 W/m<sup>2</sup> for the solar radiation, flow rate range of 0.14 to 1.27 LPM, ambient temperature range of 293 to 308K, and wind speed range of 0 to 3 m/s, which is equivalent to convection coefficient range of 2.8 to 11.8 W/m<sup>2</sup>K. The maximum average temperature of the PV module reached 318.84K with solar radiation of 1200 W/m<sup>2</sup> and a cooling flow rate of 1.27 LPM. The proposed system achieved a maximum value of temperature un-uniformity of the PV module of 3.59K under a flowrate of 1.27 LPM, and solar radiation of 1200 W/m<sup>2</sup>. This low value helps in extending the lifetime of the PV module because of the thermal stresses. For the understudy PVT system, the maximum values of thermal, electrical, and overall efficiency reached 54.43%, 14.23%, and 68.1%, respectively, which show a promising behaviour with a promising applicability in cogeneration systems. Integrated the feedforward neural network architecture with the optimization capabilities of the AHO Algorithm allows the model to achieve accurate predictions of PVT performance. The proposed FFNN-AHO hybrid model was able to minimize the MSE to a final value of 2.56×E-04 after 64 training epochs. This indicates that the model's predictions were very close to the actual values. The reliability of the proposed model's predictions was achieved where the regression factor values were very close to one for both testing and validation, as well as during the training phase. These values of the regression factor reflect the relationship between the predicted values and the actual values. So, the FFNN-AHO hybrid model was able to effectively predict the true values of performance, validation, and testing (PVT) performance. The proposed FFNN-AHO hybrid model proved effectiveness in achieving accurate predictions and demonstrating generalization and extrapolation abilities. The proposed MFFNN-AHO model exhibited superior performance compared to the other ANN models.

#### ACKNOWLEDGEMENT

The authors extend their appreciation to the deanship of scientific research at Shaqra University for funding this research work through the project number (SU-ANN-202308).




## REFERENCES

- [1] D. De Luca, A. Caldarelli, E. Gaudino, E. Di Gennaro, M. Musto, and R. Russo, "Modeling of energy and exergy efficiencies in high vacuum flat plate photovoltaic-thermal (PV-T) collectors," *Energy Reports*, vol. 9, pp. 1044–1055, Mar. 2023, doi: 10.1016/j.egy.2022.11.152.
- [2] N. S. B. Rukman, A. Fudholi, I. Taslim, M. A. Indrianti, and I. N. Manyoe, "Overview on recent photovoltaic module cooling methods: Advances PVT systems," *International Journal of Electrical and Computer Engineering*, vol. 10, no. 1, pp. 15–21, Feb. 2020, doi: 10.11591/ijece.v10i1.pp15-21.
- [3] A. Fudholi *et al.*, "Overview of photovoltaic thermal (PVT) water collector," *International Journal of Power Electronics and Drive Systems*, vol. 9, no. 4, pp. 1891–1898, Dec. 2018, doi: 10.11591/ijpeds.v9.i4.pp1891-1898.
- [4] F. Bayrak, H. F. Oztop, and F. Selimefendigil, "Effects of different fin parameters on temperature and efficiency for cooling of photovoltaic panels under natural convection," *Solar Energy*, vol. 188, pp. 484–494, Aug. 2019, doi: 10.1016/j.solener.2019.06.036.
- [5] E. Arslan, M. Aktaş, and Ö. F. Can, "Experimental and numerical investigation of a novel photovoltaic thermal (PV/T) collector with the energy and exergy analysis," *Journal of Cleaner Production*, vol. 276, 2020, doi: 10.1016/j.jclepro.2020.123255.
- [6] J. G. Hernandez-Perez, J. G. Carrillo, A. Bassam, M. Flota-Banuelos, and L. D. Patino-Lopez, "Thermal performance of a discontinuous finned heatsink profile for PV passive cooling," *Applied Thermal Engineering*, vol. 184, p. 116238, Feb. 2021, doi: 10.1016/j.applthermaleng.2020.116238.
- [7] M. R. Goma, W. Hammad, M. Al-Dhaifallah, and H. Rezk, "Performance enhancement of grid-tied PV system through proposed design cooling techniques: An experimental study and comparative analysis," *Solar Energy*, vol. 211, pp. 1110–1127, Nov. 2020, doi: 10.1016/j.solener.2020.10.062.
- [8] N. A. S. Elminshawy, A. M. I. Mohamed, K. Morad, Y. Elhenawy, and A. A. Alrobaian, "Performance of PV panel coupled with geothermal air cooling system subjected to hot climatic," *Applied Thermal Engineering*, vol. 148, pp. 1–9, Feb. 2019, doi: 10.1016/j.applthermaleng.2018.11.027.
- [9] U. J. Rajput and J. Yang, "Comparison of heat sink and water type PV/T collector for polycrystalline photovoltaic panel cooling," *Renewable Energy*, vol. 116, pp. 479–491, Feb. 2018, doi: 10.1016/j.renene.2017.09.090.
- [10] P. Bevilacqua, R. Bruno, and N. Arcuri, "Comparing the performances of different cooling strategies to increase photovoltaic electric performance in different meteorological conditions," *Energy*, vol. 195, 2020, doi: 10.1016/j.energy.2020.116950.
- [11] M. Lebbi *et al.*, "Energy performance improvement of a new hybrid PV/T Bi-fluid system using active cooling and self-cleaning: Experimental study," *Applied Thermal Engineering*, vol. 182, p. 116033, Jan. 2021, doi: 10.1016/j.applthermaleng.2020.116033.
- [12] W. Pang, Y. Zhang, B. C. Duck, H. Yu, X. Song, and H. Yan, "Cross sectional geometries effect on the energy efficiency of a photovoltaic thermal module: Numerical simulation and experimental validation," *Energy*, vol. 209, p. 118439, Oct. 2020, doi: 10.1016/j.energy.2020.118439.
- [13] C. Shen, Y. Zhang, C. Zhang, J. Pu, S. Wei, and Y. Dong, "A numerical investigation on optimization of PV/T systems with the field synergy theory," *Applied Thermal Engineering*, vol. 185, p. 116381, Feb. 2021, doi: 10.1016/j.applthermaleng.2020.116381.
- [14] A. Hassan *et al.*, "An experimental and numerical study on the impact of various parameters in improving the heat transfer performance characteristics of a water based photovoltaic thermal system," *Renewable Energy*, vol. 202, pp. 499–512, Jan. 2023, doi: 10.1016/j.renene.2022.11.087.
- [15] M. R. Kalateh, A. Kianifar, and M. Sardarabadi, "Energy, exergy, and entropy generation analyses of a water-based photovoltaic thermal system, equipped with clockwise counter-clockwise twisted tapes: An indoor experimental study," *Applied Thermal Engineering*, vol. 215, p. 118906, Oct. 2022, doi: 10.1016/j.applthermaleng.2022.118906.
- [16] W. Chiang, I. Permana, F. Wang, H. Chen, and M. Erdenebayar, "Experimental investigation for an innovative hybrid photovoltaic/Thermal (PV/T) solar system," *Energy Reports*, vol. 8, pp. 910–918, Nov. 2022, doi: 10.1016/j.egy.2022.10.264.
- [17] G. S. Menon, S. Murali, J. Elias, D. S. Aniesrani Delfiya, P. V. Alfia, and M. P. Samuel, "Experimental investigations on unglazed photovoltaic-thermal (PVT) system using water and nanofluid cooling medium," *Renewable Energy*, vol. 188, pp. 986–996, Apr. 2022, doi: 10.1016/j.renene.2022.02.080.
- [18] Z. Han, K. Liu, G. Li, X. Zhao, and S. Shittu, "Electrical and thermal performance comparison between PVT-ST and PV-ST systems," *Energy*, vol. 237, p. 121589, Dec. 2021, doi: 10.1016/j.energy.2021.121589.
- [19] A. Kazemian, M. Khatibi, T. Ma, J. Peng, and Y. Hongxing, "A thermal performance-enhancing strategy of photovoltaic thermal systems by applying surface area partially covered by solar cells," *Applied Energy*, vol. 329, 2023, doi: 10.1016/j.apenergy.2022.120209.
- [20] Z. Song, Y. Xue, B. Jia, and Y. He, "Introduction of the rectangular hole plate in favor of the performance of photovoltaic thermal solar air heaters with baffles," *Applied Thermal Engineering*, vol. 220, 2023, doi: 10.1016/j.applthermaleng.2022.119774.
- [21] H. Choi and K. Choi, "Parametric study of a novel air-based photovoltaic-thermal collector with a transverse triangular-shaped block," *Renewable Energy*, vol. 201, pp. 96–110, Dec. 2022, doi: 10.1016/j.renene.2022.10.056.
- [22] N. S. Nazri, A. Fudholi, M. H. Ruslan, and K. Sopian, "Experimental study of photovoltaic thermal-thermoelectric (PVT-TE) air collector," *International Journal of Power Electronics and Drive Systems*, vol. 9, no. 3, pp. 1390–1396, Sep. 2018, doi: 10.11591/ijpeds.v9.i3.pp1390-1396.
- [23] S. Diwania, M. Kumar, R. Kumar, A. Kumar, V. Gupta, and P. Khetrapal, "Machine learning-based thermo-electrical performance improvement of nanofluid-cooled photovoltaic-thermal system," *Energy and Environment*, p. 0958305X2211469, Dec. 2022, doi: 10.1177/0958305X221146947.
- [24] H. Kalani, M. Sardarabadi, and M. Passandideh-Fard, "Using artificial neural network models and particle swarm optimization for manner prediction of a photovoltaic thermal nanofluid based collector," *Applied Thermal Engineering*, vol. 113, pp. 1170–1177, Feb. 2017, doi: 10.1016/j.applthermaleng.2016.11.105.
- [25] W. Wang, M. Li, R. H. E. Hassanien, M. e. Ji, and Z. Feng, "Optimization of thermal performance of the parabolic trough solar collector systems based on GA-BP neural network model," *International Journal of Green Energy*, vol. 14, no. 10, pp. 819–830, Aug. 2017, doi: 10.1080/15435075.2017.1333433.
- [26] S. Delfani, M. Esmaeili, and M. Karami, "Application of artificial neural network for performance prediction of a nanofluid-based direct absorption solar collector," *Sustainable Energy Technologies and Assessments*, vol. 36, 2019, doi: 10.1016/j.seta.2019.100559.
- [27] J. H. Yousif, H. A. Kazem, N. N. Alattar, and I. I. Elhassan, "A comparison study based on artificial neural network for assessing PV/T solar energy production," *Case Studies in Thermal Engineering*, vol. 13, 2019, doi: 10.1016/j.csite.2019.100407.
- [28] A. H. A. Al-Waeli, H. A. Kazem, J. H. Yousif, M. T. Chaichan, and K. Sopian, "Mathematical and neural network modeling for predicting and analyzing of nanofluid-nano PCM photovoltaic thermal systems performance," *Renewable Energy*, vol. 145, pp. 963–980, Jan. 2020, doi: 10.1016/j.renene.2019.06.099.




- [29] O. Büyükalaca, H. M. Kılıç, U. Olmuş, Y. E. Güzelel, and K. N. Çerçi, "Numerical investigation and ANN modeling of performance for hexagonal boron Nitride-water nanofluid PVT collectors," *Thermal Science and Engineering Progress*, vol. 43, p. 101997, Aug. 2023, doi: 10.1016/j.tsep.2023.101997.
- [30] Y. Chaibi, M. Malvoni, T. El Rhafiki, T. Kousksou, and Y. Zeraoui, "Artificial neural-network based model to forecast the electrical and thermal efficiencies of PVT air collector systems," *Cleaner Engineering and Technology*, vol. 4, p. 100132, Oct. 2021, doi: 10.1016/j.clet.2021.100132.
- [31] Y. Cao, E. Kamrani, S. Mirzaei, A. Khandakar, and B. Vaferi, "Electrical efficiency of the photovoltaic/thermal collectors cooled by nanofluids: Machine learning simulation and optimization by evolutionary algorithm," *Energy Reports*, vol. 8, pp. 24–36, Nov. 2022, doi: 10.1016/j.egy.2021.11.252.
- [32] A. Nahar, M. Hasanuzzaman, and N. A. Rahim, "Numerical and experimental investigation on the performance of a photovoltaic thermal collector with parallel plate flow channel under different operating conditions in Malaysia," *Solar Energy*, vol. 144, pp. 517–528, Mar. 2017, doi: 10.1016/j.solener.2017.01.041.
- [33] A. Inc, "FLUENT 14.5 User's guid." 2015.
- [34] A. Tiwari, M. S. Sodha, A. Chandra, and J. C. Joshi, "Performance evaluation of photovoltaic thermal solar air collector for composite climate of India," *Solar Energy Materials and Solar Cells*, vol. 90, no. 2, pp. 175–189, Jan. 2006, doi: 10.1016/j.solmat.2005.03.002.
- [35] E. M. Abo-Zahhad, S. Ookawara, A. Radwan, A. H. El-Shazly, and M. F. ElKady, "Thermal and structure analyses of high concentrator solar cell under confined jet impingement cooling," *Energy Conversion and Management*, vol. 176, pp. 39–54, Nov. 2018, doi: 10.1016/j.enconman.2018.09.005.
- [36] M. A. Essa, A. A. Alshqirate, and A. Y. Hatata, "Analyzing the effect of normally distributed cooling channels on a photovoltaic thermal solar unit," *Journal of Cleaner Production*, vol. 426, 2023, doi: 10.1016/j.jclepro.2023.139015.
- [37] N. Leema, H. K. Nehemiah, and A. Kannan, "Neural network classifier optimization using differential evolution with global information and back propagation algorithm for clinical datasets," *Applied Soft Computing Journal*, vol. 49, pp. 834–844, Dec. 2016, doi: 10.1016/j.asoc.2016.08.001.
- [38] F. Zitouni, S. Harous, A. Belkeram, and L. E. B. Hammou, "The archerfish hunting optimizer: a novel metaheuristic algorithm for global optimization," *Arabian Journal for Science and Engineering*, vol. 47, no. 2, pp. 2513–2553, Feb. 2022, doi: 10.1007/s13369-021-06208-z.
- [39] V. Desika Vinayaki and R. Kalaiselvi, "AHO-MLCNN: archerfish hunting optimisation based modified lightweight CNN for diabetic retinopathy detection," *Computer Methods in Biomechanics and Biomedical Engineering: Imaging and Visualization*, vol. 11, no. 5, pp. 1937–1946, Sep. 2023, doi: 10.1080/21681163.2023.2203262.

## BIOGRAPHIES OF AUTHORS






**Mohamed A. Essa**    received his BSc in mechanical power engineering from Zagazig University, Egypt in 2004. Then he got his Bsc., and Ph.D., degrees in mechanical engineering from Polytechnique University of Valencia in 2009 and 2013, respectively. Associate Professor of Mechanical Engineering Department of Mechanical Engineering, Shaqra University, KSA. Department of Mechanical Power Engineering, Faculty of Engineering, Zagazig University, 44519 Zagazig, Egypt. The fields of interest are: turbulent flows modelling and simulation, PCMs, solar heating and desalination, ETSC, and PVT. He can be contacted at email: maessa@su.edu.sa.



**Prof. Dr. Alaa M. Rashad**    is a Professor at the Building Materials and Quality Control Institute, Housing and Building National Research Center (HBRC), Cairo, Egypt as well as the Civil Engineering Department, College of Engineering, Shaqra University, Al-Dawadmi, Riyadh, Saudi Arabia. He received his B.S., M.S., and Ph.D. from the Faculty of Engineering, Cairo University, Cairo, Egypt. He received his Post-doctoral Research Associate from the School of Planning, Architecture, and Civil Engineering, Queen's University Belfast, United Kingdom. His research interests include building materials, nanotechnology, alkali-activated materials, fire resistance, and thermal insulation. He can be contacted at email: a.rashad@su.edu.sa.



**Prof. Dr. Ahmed Y. Hatata**    received the B.S., M.S., and Ph.D. degrees from the Department of Electrical Engineering, Faculty of Engineering, Mansoura University, Egypt, in 2002, 2007, and 2012, respectively. In 2012, he became an Assistant Professor at Mansoura University, and an Associate Professor, in 2019. He is currently working as an Associate Professor with the College of Engineering, Shaqra University, Saudi Arabia. His research interests include operation, control, and protection of distribution systems, power quality, power system optimization, renewable energy sources, micro grids, and smart grids. He can be contacted at email: ahmed\_hatata@su.edu.sa.